remote sensing

MDPI

Technical Note

Bandlimited Frequency-Constrained Iterative Methods

Harrison Garrett and David G. Long *

Electrical and Computer Engineering Department, Brigham Young University, Provo, UT 84602, USA; hcgarret@byu.edu
* Correspondence: long@ee.byu.edu

Abstract: Variable aperture sampling reconstruction matrices have a history of being computationally intensive due to the need to compute a full matrix inverse. In the field of remote sensing, several spaceborne radiometers and scatterometers, which have irregular sampling and variable apertures, use iterative techniques to reconstruct measurements of the Earth's surface. However, many of these iterative techniques tend to over-amplify noise features outside the reconstructable bandwidth. Because the reconstruction of discrete samples is inherently bandlimited, solving a bandlimited inverse can focus on recovering signal features and prevent the over-amplification of noise outside the signal bandwidth. To approximate a bandlimited inverse, we apply bandlimited constraints to several well-known iterative reconstruction techniques: Landweber iteration, additive reconstruction technique (ART), Richardson–Lucy iteration, and conjugate gradient descent. In the context of these iterative techniques, we derive an iterative method for inverting variable aperture samples, taking advantage of the regular and irregular content of variable apertures. We find that this iterative method for variable aperture reconstruction is equivalent to solving a bandlimited conjugate gradient descent algorithm.

Keywords: iterative inverse; bandlimited; resolution enhancement; variable apertures; conjugate gradient descent

1. Introduction

Reconstructing an image or signal from a set of discrete measurements can be generalized as computing an inverse of the sampling matrix [1]. While there is an abundance of matrix inversion methods that can be used to perform reconstruction, the complexity of computing a direct inverse quickly prevents these reconstruction methods from being practical. However, in the case of uniform sampling and constant measurement apertures, the sampling matrix takes on a Toeplitz structure. This means that its inverse can be computed using fast Fourier transform (FFT) deconvolution techniques. When measurements are not uniform or have variable aperture measurements, re-sampling and interpolation techniques have been used to approximate a sampling matrix with a Toeplitz matrix [2].

When these techniques take on too much computational complexity, other methods are needed to compute the sampling matrix inverse. Iterative matrix inversion methods are often the preferred reconstruction method, as they typically require less computation to approximate a matrix inverse. Example iterative matrix inverse methods include Landweber iteration, algebraic reconstruction techniques (ARTs), Richardson–Lucy iteration, and conjugate gradient descent algorithms. Each one of these methods has a different iteration start, step size, and noise response.

In the field of remote sensing, several spaceborne radiometers and scatterometers have irregular or variable apertures and rely on these iterative techniques and other inversion

Academic Editor: Dusan Gleich

Received: 22 November 2024
Revised: 6 January 2025
Accepted: 8 January 2025
Published: 10 January 2025

Citation: Garrett, H.; Long, D. Bandlimited Frequency-Constrained Iterative Methods. *Remote Sens.* **2025**, *17*, 236. https://doi.org/10.3390/rs17020236

methods to perform measurement reconstruction of the Earth's surface [3–5]. Since each method uses different constraints and has different regularization tradeoffs, it can be hard to know which algorithm's constraints or regularization methods are ideal for reconstructing a given set of variable aperture measurements. Instead of contrasting the differences between these various iterative methods, we address how these methods approach a bandlimited inverse under bandlimited sampling assumptions. A bandlimited inverse is ideal for the reconstruction of variable aperture measurements as discussed in [6]. We focus on applying three bandlimiting modifications: adjusting the starting point of iteration with a deconvolution, adding a bandlimited constraint to each iteration step, and incrementing the bandlimit of each iteration.

In this paper, we introduce a bootstrapping method for handling irregularly spaced variable aperture measurements, which splits the inverse computation into uniform deconvolution and variable aperture reconstruction steps. The uniform step performs deconvolution with an FFT, and the variable and irregular apertures are reconstructed iteratively. To motivate this method, we first review the example iterative methods mentioned previously, highlighting the aforementioned bandlimiting modifications.

2. Materials and Methods

To ensure consistent notation, we define a discrete sampling system as

$$\mathbf{y} = \mathbf{M}\mathbf{x} + \boldsymbol{\nu}, \tag{1}$$

where $\mathbf{x}$ is a discrete signal or image of length N, $\mathbf{y}$ is a vector of M discrete measurements, $\boldsymbol{\nu}$ is a vector of measurement noise, and $\mathbf{M}$ is the $[M \times N]$ sampling matrix modeling each measurement as a weighted average of $\mathbf{x}$. Solving for, or approximating, the inverse of $\mathbf{M}$ generalizes the process of signal or image reconstruction, as follows:

$$\hat{\mathbf{x}} = \mathbf{M}^{\dagger}\mathbf{y}, \tag{2}$$

where $\hat{\mathbf{x}}$ is the approximation or reconstruction of $\mathbf{x}$, and $\mathbf{M}^{\dagger}$ is the generalized inverse of $\mathbf{M}$.

While a generalized inverse can be used to reconstruct and parse the overlap between measurements and their apertures, sampling theory provides more efficient techniques given specific sampling requirements [1]. Sampling matrices comprising regularly spaced samples and fixed apertures can be solved readily with matrix deconvolution techniques. Irregular apertures require more inverse considerations, which other sampling-based reconstruction methods can provide [7]. One common feature of the relationship between matrix inversion methods and sampling theory is that the number of independent samples limits the reconstructable frequency content, or rank, of the sampling matrix. This concept leads to a generalization that there is a bandlimit of reconstruction, or limit to the reconstructable frequency content, found in the inverse of a sampling matrix, i.e., a bandlimited sampling matrix inverse [8]. Under bandlimited assumptions, the generalized inverse solution in Equation (2) can be modified to be a bandlimited inverse [6] using a bandlimited projection matrix $\mathbf{B}$, as follows:

$$\hat{\mathbf{x}} = (\mathbf{B}\mathbf{M})^{\dagger}\mathbf{y}. \tag{3}$$

In this paper, we focus on how existing iterative methods can be constrained to solve Equation (2) using a bandlimited deconvolution preconditioner $\mathbf{A}^{\dagger}$, such that $\mathbf{A}\mathbf{A}^{\dagger} = \mathbf{B}$, and using additional bandlimited step constraints ($\mathbf{B}_n$ for each nth iteration). A more detailed derivation of a bandlimited inverse and its connection to sampling theory is given in [6]. We now review some well-known iterative reconstruction techniques and how they relate to approximating the generalized inverse in Equation (2). Following this review, we introduce the three bandlimiting modifications using a bandlimited deconvolution preconditioner and additional step constraints. Using these modifications, we arrive at an iterative method for variable aperture reconstruction.

2.1. Landweber Iteration

Landweber iteration [9] is a special case of gradient descent, where each iteration takes a step in the opposite direction of the projected measurement error, as follows:

$$\hat{\mathbf{x}}_{n+1} = \hat{\mathbf{x}}_n + \lambda \mathbf{M}^*(\mathbf{y} - \mathbf{M}\hat{\mathbf{x}}_n), \tag{4}$$

where $\hat{\mathbf{x}}_n$ is the nth iteration step, and λ is a step size scalar used to control convergence. If we initialize $\hat{\mathbf{x}}_0$ as the zero vector $\mathbf{0}$, we can solve for the nth iteration of the Landweber iteration as

$$\hat{\mathbf{x}}_n = \left[\sum_{i=0}^{n} (\mathbf{I} - \lambda \mathbf{M}^*\mathbf{M})^i\right] \lambda \mathbf{M}^*\mathbf{y}. \tag{5}$$

If all the eigenvalues of $(\mathbf{I} - \lambda \mathbf{M}^*\mathbf{M})$ are less than 1, then the Landweber solution theoretically converges to the pseudo-inverse of $\mathbf{M}$ so that at $n = \infty$,

$$\hat{\mathbf{x}}_\infty = (\mathbf{M}^*\mathbf{M})^\dagger \mathbf{M}^*\mathbf{y}. \tag{6}$$

While Landweber iteration appears simple and theoretically converges to a well-known result, the starting step $\lambda\mathbf{M}^*\mathbf{y}$ may be far away from the final solution, and the step size λ required for convergence may require an impractical amount of iterations. Furthermore, each iteration step can be sensitive to the noise found within $\mathbf{y}$, causing small errors to accumulate and skew the converged solution farther away from the true solution (this behavior is called semi-convergence [10], or noise amplification in other inverse processes).

To mitigate these issues, both preconditioning and step size constraints can be used at each iteration to regularize the measurement noise and alter the point of convergence. The use of a preconditioner and regularizer to reconstruct variable aperture measurements can be found in [11,12]. A preconditioning matrix $\mathbf{R}$ and a step constraint $\mathbf{H}$ can be incorporated into each Landweber iteration as

$$\hat{\mathbf{x}}_{n+1} = \hat{\mathbf{x}}_n + \lambda \mathbf{H}\mathbf{M}^*\mathbf{R}(\mathbf{y} - \mathbf{M}\hat{\mathbf{x}}_n). \tag{7}$$

Given that the effect of $\mathbf{H}$ is dependent on the structure of $\mathbf{M}$ and the nature of $\mathbf{y}$, the ideal choice of step constraint and stopping rules is a wide field of study [13]. However, under bandlimited sampling assumptions, we make the claim that bandlimited step constraints are ideal for variable aperture reconstruction. This is further expanded on in later sections. To understand why other step constraints can be chosen as optimal, an assertion on the bandlimited convergence of iterative step constraints is given in Appendix A.

2.2. Algebraic Reconstruction Technique

To allow each measurement to individually influence the iteration step, the algebraic reconstruction technique (ART) updates each projected measurement error separately and adds a normalization to each update [14], as follows:

$$\hat{x}_{n+1,k} = \hat{x}_n + \frac{\lambda\, m_{ik}}{\sum_l m_{il}^*\, m_{il}} (z_i - \sum_l m_{il}\, \hat{x}_{nl}), \tag{8}$$

where z_i is the ith measurement, $\hat{x}_{nk}$ is the kth element $\hat{\mathbf{x}}_n$, and m_{ik} is each element of $\mathbf{M}$. A simultaneous, or block, version of ART can be formed by waiting to apply all measurement ART updates at the same time, as follows:

$$\hat{\mathbf{x}}_{n+1} = \hat{\mathbf{x}}_n + \mathbf{\Lambda}\mathbf{M}^*(\mathbf{y} - \mathbf{M}\hat{\mathbf{x}}_n),$$
$$\mathbf{\Lambda} = \lambda \begin{bmatrix} \|\mathbf{m}_0\|^{-2} & \dots & 0 \\ 0 & \|\mathbf{m}_1\|^{-2} & 0 \\ \dots & \dots & \|\mathbf{m}_n\|^{-2} \end{bmatrix} \tag{9}$$

where block ART is a special case of a normalized Landweber iteration when the normalization Λ is included in the step constraint. This normalization helps put each measurement projection on the same scale so that one measurement update does not skew the iteration process. Note that the starting iteration of block ART is equivalent to the backprojection $\hat{\mathbf{x}}_0 = \mathbf{M}^*\mathbf{y}$ normalized by the magnitude of each measurement response Λ.

2.3. Richardson–Lucy

Instead of an additive update, the Richardson–Lucy [15,16] method uses a multiplicative update and projected error ratio, as follows:

$$\hat{x}_{0,k} = \frac{\sum_i m_{ik}^* z_i}{\sum_j m_{jk}^*},$$
$$\hat{x}_{n+1,k} = \sum_{ijl} \frac{m_{ik}^* z_i \hat{x}_{nk}}{m_{jk}^* m_{il} \hat{x}_{nl}}, \tag{10}$$

where i and j are indices over each measurement, and k and l are indices over each value in $\hat{\mathbf{x}}_n$. The starting point is similar to the block ART method, being the backprojection $\mathbf{M}^*\mathbf{y}$ normalized by the sum of measurement responses at each point in $\hat{\mathbf{x}}$. If $\mathbf{M}$ is circulant, then the normalization is equivalent to a scale factor (i.e., same scale on each column of $\mathbf{M}^*$). While the multiplicative nature of each iteration makes a proof of convergence difficult, it has been shown that if the iteration converges, it converges to a maximum likelihood solution [17].

2.4. Conjugate Gradient

To limit the total number of iterations and control the convergence, orthogonalization of each iteration's error can be performed. A method that uses orthogonal error steps is conjugate gradient descent (CG). Because the conjugate gradient method requires the sampling matrix to be symmetric, we summarize the conjugate gradient method using unique variable names for the symmetric sampling matrix ($\mathbf{\Lambda}$), its corresponding measurements ($\mathbf{d}$), and its conjugate directions ($\mathbf{c}_n$).

If each iteration's measurement error is $\mathbf{r}_n$, then $\mathbf{r}_i^*\mathbf{r}_j = 0,\ \forall i \neq j$ means each iteration error is orthogonal to all other iterations. When the sampling matrix is symmetric ($\mathbf{\Lambda}^* = \mathbf{\Lambda}$) and positive definite, the CG method can be used to iterate in conjugate steps (i.e., orthogonal with respect to $\mathbf{\Lambda}$). If $\mathbf{c}_n$ is the direction of each iteration step, then for each step to be conjugate to all other steps, $\mathbf{c}_i^*\mathbf{\Lambda}\mathbf{c}_j = 0,\ \forall i \neq j$. The conjugate gradient method can be implemented by orthogonalizing each step's direction with respect to $\mathbf{\Lambda}$, as follows:

$$\mathbf{r}_n = (\mathbf{d} - \mathbf{\Lambda}\hat{\mathbf{g}}_n),$$
$$\mathbf{c}_n = \mathbf{r}_n - \sum_{i=0}^{n-1} \frac{\mathbf{c}_i^*\mathbf{\Lambda}\mathbf{r}_n}{\mathbf{c}_i^*\mathbf{\Lambda}\mathbf{c}_i}\mathbf{c}_i, \tag{11}$$
$$\hat{\mathbf{g}}_{n+1} = \hat{\mathbf{g}}_n + \frac{\mathbf{c}_n^*\mathbf{r}_n}{\mathbf{c}_n^*\mathbf{\Lambda}\mathbf{c}_n}\mathbf{c}_n,$$

where $\mathbf{r}_n$ is each step's predicted measurement error, $\mathbf{c}_n$ is each step's conjugate direction, and $\hat{\mathbf{g}}_n$ is the *symmetric* iterative solution.

While the convergence of CG is limited to matrices that are symmetric and positive definite, variations of CG such as the bi-conjugate or the generalized minimal residual methods can further generalize these constraints [18,19].

2.5. Separating Regular and Irregular Apertures

To introduce the use of a bandlimited deconvolution preconditioner, we first take advantage of the common structure often found in sampling matrices by separating the sampling matrix $\mathbf{M}$ into two parts: an averaged regularly sampled constant aperture $\mathbf{A}$ and irregular aperture perturbations $\mathbf{P}$, where $\mathbf{M} = (\mathbf{A} + \mathbf{P})$.

Theoretically, any $\mathbf{A}$ can be chosen for this separation; however, if the pseudo-inverse of $\mathbf{A}$ is used as a preconditioner of the sampling matrix inverse, i.e., $\mathbf{M}^\dagger = \mathbf{A}^\dagger(\mathbf{M}\mathbf{A}^\dagger)^\dagger$, then the choice of $\mathbf{A}^\dagger$ may speed up the computation of $\mathbf{M}^\dagger$. Additionally, the choice of $\mathbf{A}^\dagger$ can be used to bandlimit the computation of $\mathbf{M}^\dagger$. To show these advantages, we use the Woodbury matrix inversion lemma [20]. A reduced form of this lemma is

$$(\mathbf{A} + \mathbf{P})^{-1} = \mathbf{A}^{-1} - \mathbf{A}^{-1}(\mathbf{I} + \mathbf{P}\mathbf{A}^{-1})^{-1}\mathbf{P}\,\mathbf{A}^{-1}, \tag{12}$$

where $\mathbf{A}$ is full rank, $\mathbf{P}$ consists of k-rank updates to $\mathbf{A}$, and $(\mathbf{I} - \mathbf{P}\mathbf{A}^{-1})^{-1} = \mathbf{C}$ is called the capacitance matrix. Since the lemma above assumes that both $\mathbf{A}$ and $\mathbf{C}$ are invertible matrices, we rely on a more generalized solution [21] using rank-limited pseudo-inverses of $\mathbf{A}$ and $\mathbf{C}$, as follows:

$$(\mathbf{B}\mathbf{M})^\dagger = (\mathbf{B}\mathbf{A} + \mathbf{B}\mathbf{P})^\dagger = \mathbf{A}^\dagger - \mathbf{A}^\dagger(\mathbf{B} + \mathbf{P}\mathbf{A}^\dagger)^\dagger\mathbf{P}\mathbf{A}^\dagger, \tag{13}$$

where $\mathbf{B} = \mathbf{A}\mathbf{A}^\dagger$ is a bandlimited projection matrix. An example of how to compute the direct solution to a rank-limited capacitance matrix can be found in [22].

Substituting Equation (13) into Equation (3), we can separate the solution to a bandlimited reconstruction into the following two parts:

$$\begin{aligned} \hat{\mathbf{x}} &= \hat{\mathbf{x}}_r - \hat{\mathbf{x}}_i, \\ \hat{\mathbf{x}}_r &= \mathbf{A}^\dagger\mathbf{y}, \\ \hat{\mathbf{x}}_i &= \mathbf{A}^\dagger(\mathbf{B} + \mathbf{P}\mathbf{A}^\dagger)^\dagger\mathbf{P}\mathbf{A}^\dagger\mathbf{y}, \end{aligned} \tag{14}$$

where $\hat{\mathbf{x}}_r$ is a regular sampling solution bandlimited by $\mathbf{A}^\dagger$, and $\hat{\mathbf{x}}_i$ is the accumulated bandlimited error found in $\hat{\mathbf{x}}_r$ due to the irregular apertures in $\mathbf{P}$, i.e., the irregular aperture corrections. As both $\hat{\mathbf{x}}_r$ and $\hat{\mathbf{x}}_i$ are bandlimited by $\mathbf{A}^\dagger$, the solution $\hat{\mathbf{x}}$ is also bandlimited. A simpler way to express $\hat{\mathbf{x}}_i$ without the need to directly compute $\mathbf{P}$ is

$$\hat{\mathbf{x}}_i = \hat{\mathbf{x}}_r - \mathbf{A}^\dagger(\mathbf{M}\mathbf{A}^\dagger)^\dagger\mathbf{y}. \tag{15}$$

If $\mathbf{A}^\dagger$ can be easily and quickly computed, the computational load of computing a bandlimited $\mathbf{M}^\dagger$ falls on solving the inverse of the capacitance matrix $(\mathbf{B} + \mathbf{P}\mathbf{A}^\dagger)^\dagger = (\mathbf{M}\mathbf{A}^\dagger)^\dagger$. Thus, choosing $\mathbf{A}^\dagger$, which can be computed efficiently and reduce the rank of $\mathbf{P}$, becomes advantageous when inverting variable aperture sampling matrices.

2.6. Bandlimited Deconvolution Preconditioner

Under bandlimited sampling theory, both irregular and regular sampling configurations are functionally equivalent [7]. This means that every sampling matrix $\mathbf{M}$ has an equivalent regularly sampled configuration that can perform the same reconstruction.

While finding an exactly equivalent regularly sampled configuration is not trivial and requires its own matrix inverse computation, we instead can choose $\mathbf{A}$ assumed to be 'close' to the equivalent regularly sampled counterpart of $\mathbf{M}$. Depending on how close, the choice of $\mathbf{A}$ can reduce the rank of $\mathbf{P}$. Ideally, $\mathbf{A}$, which produces the lowest rank $\mathbf{P}$, should be chosen.

As an example, we can choose $\mathbf{A}$ to be an interpolated bandlimited Toeplitz matrix, as follows:

$$\mathbf{A} = \mathbb{D}\mathbf{F}^{*}\mathrm{diag}(\mathbf{Fa})\mathbf{F}, \tag{16}$$

where $\mathbf{F}$ is an N length discrete Fourier transform (DFT) matrix, $\mathrm{diag}(\mathbf{x})$ indicates a diagonal matrix of $\mathbf{x}$, $\mathbf{Fa}$ is the DFT of the constant aperture $\mathbf{a}$, and $\mathbb{D}$ is a bandlimited interpolation matrix, whose rows comprise evenly spaced order M length N Dirichlet kernels. $\mathbb{D}\mathbf{y}$ is equivalent to performing the N point DFT of $\mathbf{y}$ and then taking the M point inverse DFT of the first M frequency components. The bandlimited inverse of $\mathbb{D}$ is $\mathbb{D}^{*}$, where $\mathbb{D}^{*}\mathbf{y}$ is equivalent to performing the M point DFT of $\mathbf{y}$, zero padding up to N, and then taking its N point inverse DFT.

Given its circulant nature, the pseudo-inverse $\mathbf{A}^{\dagger}$ of this choice of $\mathbf{A}$ can be computed quickly using deconvolution methods, and its bandlimited interpolation can be performed in the frequency domain. Using $\mathbf{A}^{\dagger}$ as the starting point, we can now iteratively reconstruct the rest of the variable aperture perturbations $\mathbf{P}$ using a variety of reduced-rank matrix inversion methods.

To visualize the use of a bandlimited deconvolution preconditioner, we give an example reconstruction of a low bandwidth signal using variable aperture measurements. The example truth signal, variable aperture measurements, regular aperture deconvolution, and irregular aperture corrections are shown in Figure 1.

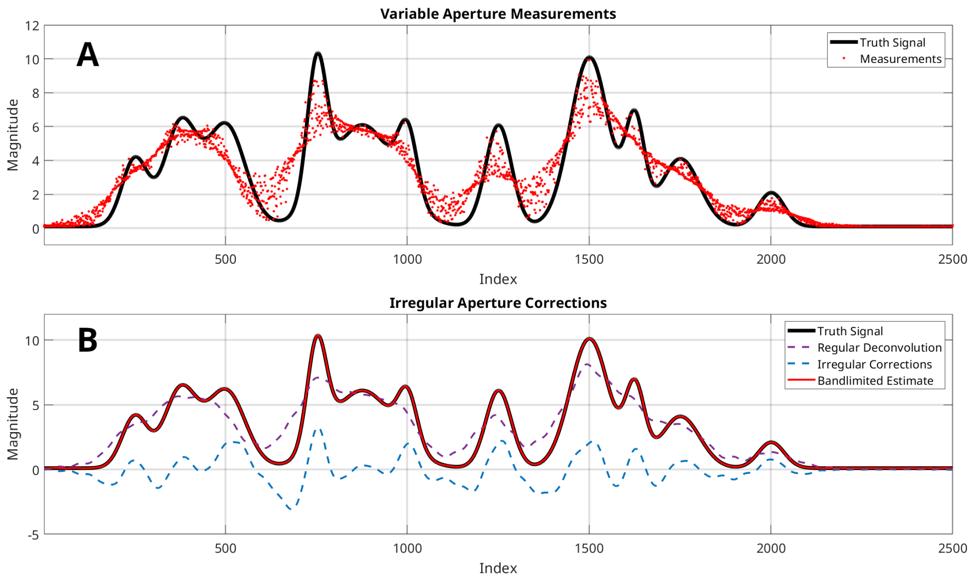

Figure 1. (**A**) Example truth signal, in black, and example variable aperture measurements, ordered by peak value, as red dots. (**B**) Example regular aperture deconvolution solution and irregular corrections iteratively found through bandlimited reconstruction. Both solutions add together to form a bandlimited estimate.

2.7. Bandlimiting Landweber-like Methods

Using $\mathbf{A}^\dagger$, we can iteratively estimate the bandlimited capacitance matrix using an approach similar to Equation (A4), assuming λ is sufficiently small, as follows:

$$(\mathbf{MA}^\dagger)^\dagger = \lambda \sum_{i=0}^{n} (\mathbf{B} - \lambda \mathbf{MA}^\dagger)^i. \tag{17}$$

Substituting Equation (17) into (14), we find the following iterative solution:

$$\begin{aligned} \hat{\mathbf{x}}_0 &= \mathbf{A}^\dagger \mathbf{y}, \\ \hat{\mathbf{x}}_{n+1} &= \hat{\mathbf{x}}_n + \lambda \mathbf{A}^\dagger (\mathbf{y} - \mathbf{M}\hat{\mathbf{x}}_n). \end{aligned} \tag{18}$$

This is a special case of Landweber iteration, which starts at $\mathbf{A}^\dagger\mathbf{y}$ and removes aliased irregular aperture perturbations in bandlimited steps. A similar frequency-filtered Landweber process is shown in [23].

Similarly, we can adjust the starting point ($\hat{\mathbf{x}}_0 = \mathbf{A}^\dagger\mathbf{y}$) and iteration steps of both ART Equation (8) and Richardson–Lucy Equation (10) iterations, respectively, as follows:

$$\hat{x}_{n+1,k} = \hat{x}_{nk} + \frac{\lambda\, a^\dagger_{ik}}{\sum_l m_{il}\, a^\dagger_{il}} (z_i - \sum_l m_{il}\, \hat{x}_{nl}), \tag{19}$$

$$\hat{x}_{n+1,k} = \sum_{ijl} \frac{a^\dagger_{ik}\, z_i\, \hat{x}_{nk}}{a^\dagger_{jk}\, m_{il}\, \hat{x}_{nl}}, \tag{20}$$

where $a^\dagger_{ik}$ is the i,kth entry of $\mathbf{A}^\dagger$. Note that in both adjustments to ART and RL, the back-projection $\mathbf{A}^*$ is replaced with $\mathbf{A}^\dagger$ and $\hat{\mathbf{x}}_n$ is limited to the bandwidth of $\mathbf{A}^\dagger$.

While the modified Landweber-like iterations in Equations (18)–(20) all theoretically converge on the bandlimited solution in Equation (A4), the number of steps and the degree of noise amplification can make this approach impractical, depending on the structure of $\mathbf{M}$ and the noise in $\mathbf{y}$.

2.8. Bandlimiting Conjugate Gradient Descent

If we make the following modifications to the inputs and outputs of the CG method in Equation (11):

$$\begin{aligned} \hat{\mathbf{g}}_0 &= \mathbf{y}, \\ \mathbf{\Lambda} &= (\mathbf{MA}^\dagger)^* \mathbf{MA}^\dagger, \\ \mathbf{d} &= (\mathbf{MA}^\dagger)^* \mathbf{y}, \\ \hat{\mathbf{x}}_n &= \mathbf{A}^\dagger \hat{\mathbf{g}}_n, \end{aligned} \tag{21}$$

we find a bandlimited CG solution to our variable aperture sampling problem, as follows:

$$\hat{\mathbf{x}}_{n+1} = \mathbf{A}^\dagger \mathbf{y} + \sum_{k=0}^{n-1} \frac{\mathbf{A}^\dagger \mathbf{c}_k \mathbf{c}_k^* \mathbf{r}_k}{\mathbf{c}_k^* \mathbf{\Lambda} \mathbf{c}_k}. \tag{22}$$

2.9. Additional Frequency Constraints

While we have shown how different iterative methods can be modified to compute a bandlimited inverse, so far, we have only placed a fixed bandlimited constraint on each iterative step $\mathbf{B} = \mathbf{AA}^\dagger$. This bandlimited constraint is implicitly made a priori by the choice and bandlimit of $\mathbf{A}^\dagger$.

To allow for more control over each inversion step, we can place a bandlimited step constraint $\mathbf{B}_n$, where $\mathbf{B}_n$ is a bandlimited projection matrix, before the application of $\mathbf{A}^\dagger$. This step constraint is placed before the preconditioner $\mathbf{A}^\dagger$ to prevent the aliasing of frequency content outside the bandlimit of each $\mathbf{B}_n$.

The ability to change the bandlimiting constraint of each iteration allows for more complex bandlimiting schemes. Of particular interest for variable aperture reconstruction is that the ability to incrementally increase the bandwidth of each $\mathbf{B}_n$ allows existing methods to solve for *incremental bandlimited solutions*, i.e., $\mathbf{M}_n^\dagger = \mathbf{A}^\dagger \mathbf{B}_n (\mathbf{M}\mathbf{A}^\dagger \mathbf{B}_n)^\dagger$. If each bandlimiting step $\mathbf{B}_n$ is strictly increasing, then, assuming sufficient iterations and conditions are taken for convergence, existing iterative methods can progressively solve each incremental bandlimited solution $\mathbf{M}_n^\dagger$ without the need to recompute a new matrix inverse. Furthermore, using additional error measures, such as a signal-to-noise ratio (SNR) test, an appropriate bandlimited inverse, one that does not extend past the inherent bandlimit of reconstruction, can be solved without determining the inherent bandlimit of reconstruction a priori. This is particularly advantageous for variable aperture sampling configurations, in which the inherent bandlimit of reconstruction can be difficult to determine.

Taking the result from Equation (22), the addition of a variable bandlimited step constraint forms a block bandlimiting CG method (BCG), as follows:

$$\hat{\mathbf{x}}_{n+1} = \mathbf{A}^\dagger \mathbf{y} + \sum_{k=0}^{n-1} \frac{\mathbf{A}^\dagger \mathbf{B}_n \mathbf{c}_k \mathbf{c}_k^* \mathbf{r}_k}{\mathbf{c}_k^* \mathbf{\Lambda} \mathbf{c}_k}. \tag{23}$$

Given the relationship between $\mathbf{c}_n$ and $\mathbf{r}_n$, the bandlimiting step constraint $\mathbf{B}_n$ can be equivalently applied directly to $\mathbf{r}_n$, i.e., $\mathbf{r}_n = \mathbf{B}_n \mathbf{r}_n$. Thus, $\mathbf{B}_n$ can also be considered a bandlimited measurement error constraint.

By reducing $\mathbf{B}_n$ to a single frequency, i.e., $\mathbf{B}_n \mathbf{r}_n = \mathbf{f}_n \mathbf{f}_n^* \mathbf{r}_n$, where $\mathbf{f}_n$ is a frequency-basis vector, we can convert the terms in Equation (22) into a frequency-basis decomposition, as follows:

$$\begin{aligned} \omega_n &= (\mathbf{f}_n^* \mathbf{r}_n)^{-1}, \\ \mathbf{f}_n &= \omega_n \mathbf{r}_n, \\ \mathbf{m}_n^\dagger &= \omega_n \mathbf{c}_n, \\ \mathbf{q}_n &= \omega_n \mathbf{M}\mathbf{A}^\dagger \mathbf{c}_n, \\ \mathbf{t}_n &= \frac{\mathbf{q}_n}{\mathbf{q}_n^* \mathbf{q}_n}, \end{aligned} \tag{24}$$

where ω_n is the inverse of the bandlimited frequency magnitude of each iteration's error. Applying these substitutions into Equation (22), we arrive at a frequency-basis BCG solution identical to the frequency-basis QR decomposition (FQR) derived in [6], as follows:

$$\hat{\mathbf{x}}_n = \sum_{k=0}^{n} \mathbf{A}^\dagger \mathbf{m}_k^\dagger \mathbf{t}_k^* \mathbf{y}. \tag{25}$$

In fact, this result indicates that the FQR method is a special case of BCG, where each iteration's error is bandlimited to a single frequency. The main difference between the two methods is that BCG projects onto conjugate directions $\mathbf{c}_i^*$, which can contain multiple frequency components, and FQR projects onto individual frequency directions $\mathbf{q}_i$. This relationship is of interest since it suggests that BCG can be used to block-update the FQR method. An example of how to perform this, with the threshold γ as a stopping constraint, is shown in Algorithm 1.

Algorithm 1 Block Frequency BCG

$\hat{\mathbf{g}}_0 \leftarrow \mathbf{y}$
$\mathbf{d} \leftarrow (\mathbf{M}\mathbf{A}^\dagger)^* \mathbf{y}$
$\mathbf{\Lambda} \leftarrow (\mathbf{M}\mathbf{A}^\dagger)^* \mathbf{M}\mathbf{A}^\dagger$
$\mathbf{r}_0 \leftarrow \mathbf{d} - \mathbf{\Lambda}\hat{\mathbf{g}}_0$
while $\|\mathbf{r}_n\| \neq 0$ **do**
  Choose a bandlimit $L = \{m, |\mathbf{r}_{nm}| > \gamma\}$
  $\mathbf{B}_n \leftarrow \sum_{m \in L} \mathbf{f}_m \mathbf{f}_m^*$
  $\mathbf{r}_n \leftarrow \mathbf{B}_n \mathbf{r}_n$
  $\mathbf{c}_n \leftarrow \mathbf{r}_n - \sum_{i=0}^{n-1} \mathbf{c}_i \mathbf{y}_i^* \mathbf{\Lambda} \mathbf{r}_n$
  $\mathbf{y}_n \leftarrow \mathbf{c}_n / (\mathbf{c}_n^* \mathbf{\Lambda} \mathbf{c}_n)$
  $\hat{\mathbf{g}}_n \leftarrow \hat{\mathbf{g}}_{n-1} + \mathbf{c}_n \mathbf{y}_n^* \mathbf{r}_n$
  $\hat{\mathbf{x}}_n \leftarrow \mathbf{A}^\dagger \hat{\mathbf{g}}_n$
  $\mathbf{r}_{n+1} \leftarrow \mathbf{d} - \mathbf{\Lambda}\hat{\mathbf{g}}_n$
  if $\left|\mathbf{r}_{(n+1)m}\right| \leq \gamma$ **then**
    $\mathbf{r}_{(n+1)m} \leftarrow 0$
  end if
end while

To reduce BCG to the original CG method, we remove both $\mathbf{A}^\dagger$ and $\mathbf{B}_n$ by replacing them with the identity matrix. Thus, BCG serves as a means to move between CG and FQR, depending on the chosen bandlimiting scheme.

2.10. Single- vs. Block-Frequency Constraints

To further contrast the choice of bandlimiting schemes, we consider the difference between FQR (single frequency), BCG (block frequency), and CG (all frequency, i.e., identity) bandlimited step constraints. Both CG and FQR methods solve the matrix inverse in a fixed number of steps. However, FQR produces a bandlimited solution solely based on the sampling matrix $\mathbf{M}$, while CG produces a non-bandlimited solution based on the averaged frequency content found in the measurements. This means that in the presence of noise, CG tends to over-amplify error outside the bandlimit of reconstruction. In contrast, the CG method may take fewer iterations to converge to a solution than the FQR method. This is because the CG method can avoid inverting frequency content not found in the measurements, while FQR requires computing over all frequency steps within the bandlimit of reconstruction. The block BCG method takes advantage of both of these strengths, while allowing for bootstrapping using the deconvolution $\mathbf{A}^\dagger$ and custom bandlimiting schemes using $\mathbf{B}_n$ in the inversion process.

3. Results

To illustrate the differences between the CG, BCG, and FQR methods, we perform simulations of a 1D truth signal using noisy and noise-free variable aperture measurements. To create the variable apertures, several skewed Gaussian apertures are used, each sampled at a random location. Example apertures, which have been reordered by their apertures' 'center' value for visual convenience, are shown in Figure 2. A short time-windowed chirp was used as the 1D truth signal shown in Figure 3, alongside an ordered set of variable aperture measurements.

Four reconstruction schemes are run in parallel using the same sampling matrix and additive measurement noise inputs. The four reconstruction schemes are the original CG and FQR methods alongside two bandlimiting schemes of BCG, a single-frequency and a block-frequency scheme. The chosen bandlimiting scheme for the block-frequency scheme consisted of block-frequency updates for the first 150 iterations, and switched to single-frequency steps thereafter (to show how BCG compromises between CG and FQR).

The simulations were repeated at 50 dB, 30 dB, and 10 dB SNR levels for each of these four algorithm variations. Additionally, all simulations were repeated using a regular sampling deconvolution step to initialize each algorithm.

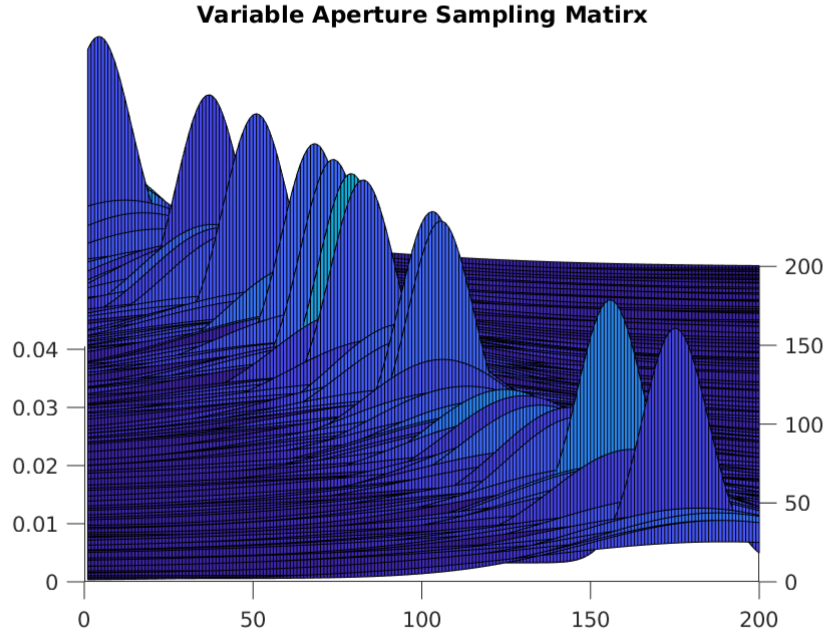

Figure 2. Example MRFs ordered by peak value centers. Note how this diagonal structure is similar to a Toeplitz matrix.

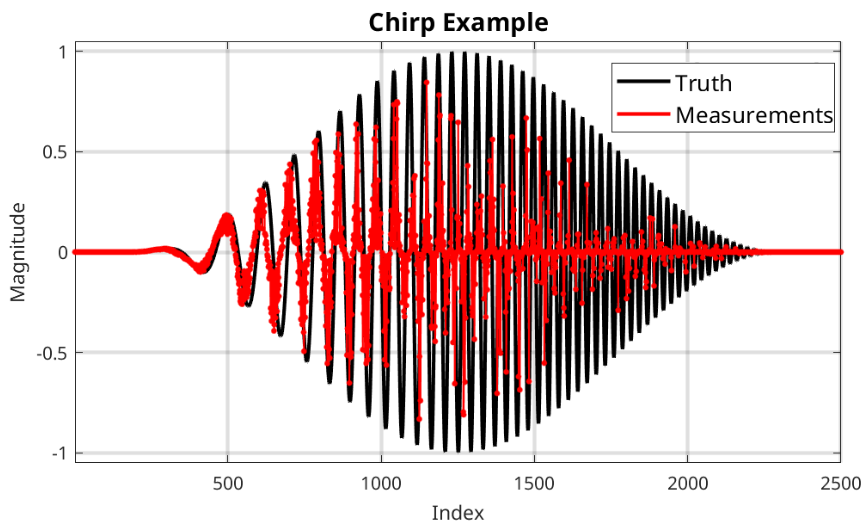

Figure 3. The short time chirp used in the simulation and the variable aperture measurements ordered by peak MRF centers.

Each method's total iteration error with respect to the truth signal is contrasted in Figure 4. In general, the deconvolution initialized solutions do not change the total error of each iteration, but do reduce the variance of each iteration step and achieve an earlier convergence. Comparing the four reconstruction schemes, the CG method appears to descend in total reconstruction error the fastest but is short-lived as the error levels out and slowly progresses until the noise overtakes the reconstruction. The FQR method appears to converge the slowest, but is able to reconstruct more of the truth signal. The BCG appears to be the compromise between FQR and CG as it converges slightly faster than FQR at first, is then slowed down by aliased content, but later catches up to FQR with single-frequency constraints. Note that as the noise level is increased, the algorithms' minimum total reconstruction error is reached earlier, after which error amplification overtakes signal reconstruction.

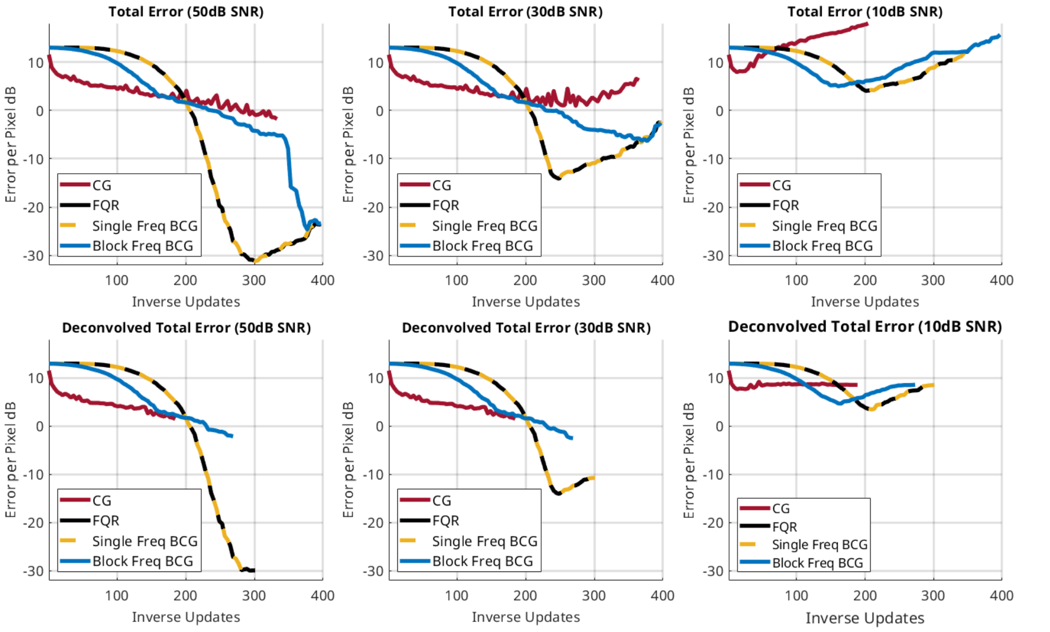

Figure 4. Total reconstruction error results for each iteration of CG, FQR, single-frequency BCG, and block-frequency BCG algorithms. Simulations are run both with and without a regular deconvolution initializer for comparison.

To better understand the trends seen in the total reconstruction results shown, we examine the frequency spectrum of the truth signal and variable aperture measurements. The discrete cosine transforms of both the truth signal and variable aperture measurements used in these simulations are shown in Figure 5. Note that the majority (greater than 99%) of the truth signal's bandwidth is contained in the first 250 DCT frequency bins. However, the variable aperture measurements possess frequency content beyond the truth signal's apparent signal bandlimit. Thus, the lowest reconstruction error occurred shortly after 250 iterations, and most algorithms began to over-amplify noise after 300 iterations.

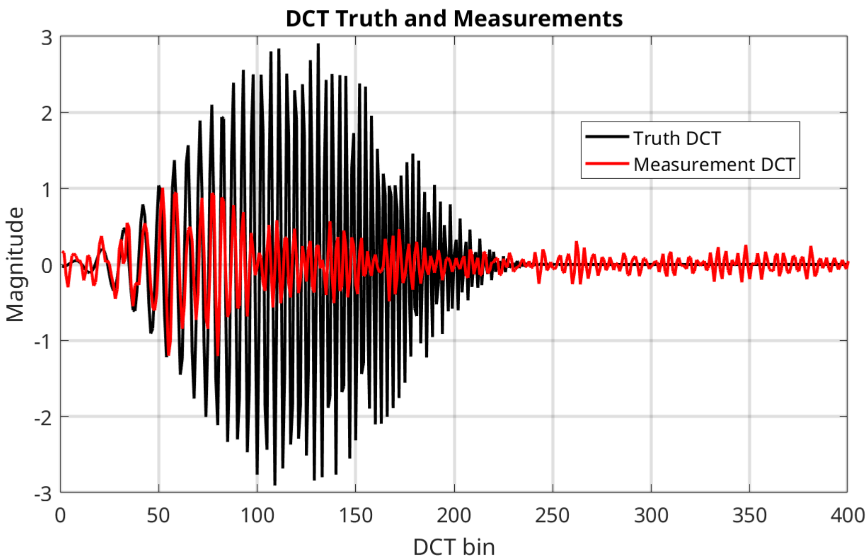

Figure 5. The discrete cosine transforms of the truth signal and variable aperture measurements to compare frequency contents. More than 99% of the truth signal is contained within 300 frequency bins. In this case, the variable aperture measurements extend past this limit.

The bandlimited nature of these algorithms can be better observed by computing the bandlimited reconstruction error of each iteration, i.e., the error with respect to the truth signal bandlimited to each iteration's frequency constraint (note that CG has no bandlimited constraint and thus is equivalent to the total error). A bandlimited error comparison is shown in Figure 6. The bandlimited error trends follow the frequency content scale seen in the DCT of the truth signal. This is because the beginning iterations have to decouple the aliasing of higher frequency content and later iterations are closer to the bandlimit of the truth signal.

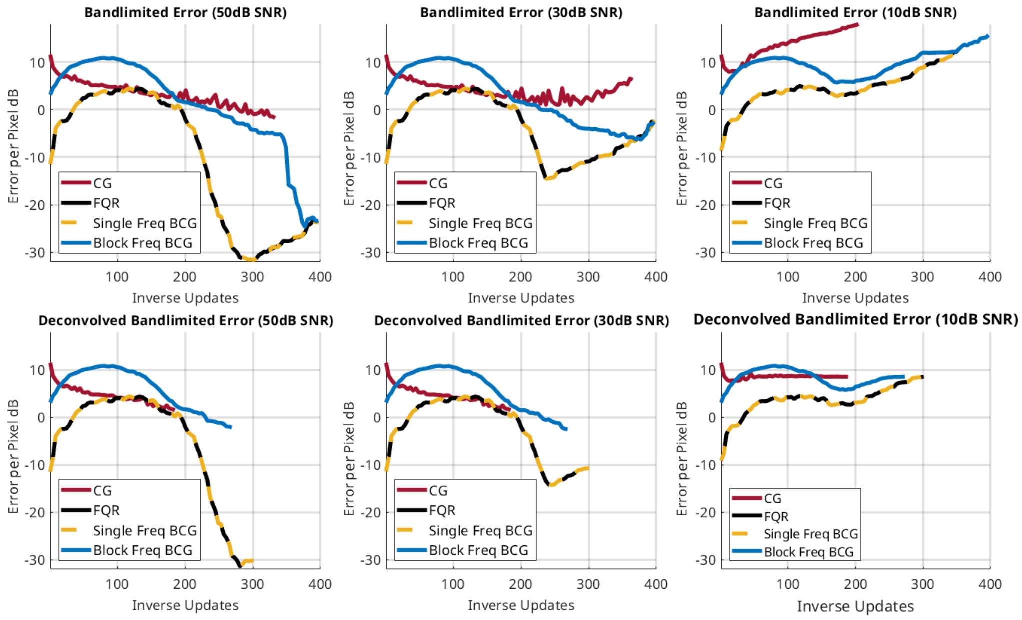

Figure 6. Bandlimited reconstruction error results for each iteration of CG, FQR, single-frequency BCG, and block-frequency BCG algorithms. Simulations are run both with and without a regular deconvolution initializer for comparison.

4. 2D Reconstruction

To provide a practical example of the resolution capabilities of BCG bandlimiting schemes, 2D simulations comparing the reconstructions of a recognizable image are made using synthetic variable Gaussian apertures. The edges of the 256 $\times$ 256 pixel truth image are tapered using an 80% Taylor window. This is performed to mitigate the poor conditioning of undersampled edges and reduce the periodic effects from bandlimited filtering. Twenty thousand 2D Gaussian ellipses with randomly chosen widths and rotations ranging from approximately 3 $\times$ 3 to 31 $\times$ 31 pixels in minimum and maximum widths, respectively, are synthetically generated to sample the truth image. Random Gaussian noise at the 0, 10, and 20 dB SNR levels with respect to the mean magnitude of the truth image is added to the synthetic variable aperture samples. All 2D simulations use the same noisy measurements and sampling apertures as inputs.

Similar to the 1D example previously shown, the three bandlimiting schemes contrasted are as follows: no step constraints (original CG), single-2D-DCT-frequency steps (equivalent to FQR), and block-frequency steps. Frequency constraints are sorted from lowest to highest frequency components in both dimensions. In place of a deconvolution preconditioner, a 4000 bin 2D DCT bandlimit is placed on the sampling apertures to reduce non-recoverable high-frequency components. To compare the over-amplification of noise, the stopping constraints are removed and a maximum of 4000 iterations are taken using each set of noisy samples and each bandlimiting scheme. Example 2D reconstructions are shown in a grid contrasting each bandlimiting scheme at various iterations at the 10 dB

SNR level; see Figure 7. The corresponding total reconstruction error and total bandlimited reconstruction error curves are shown in Figure 8 alongside 20 dB and 0 dB SNR noisy measurements.

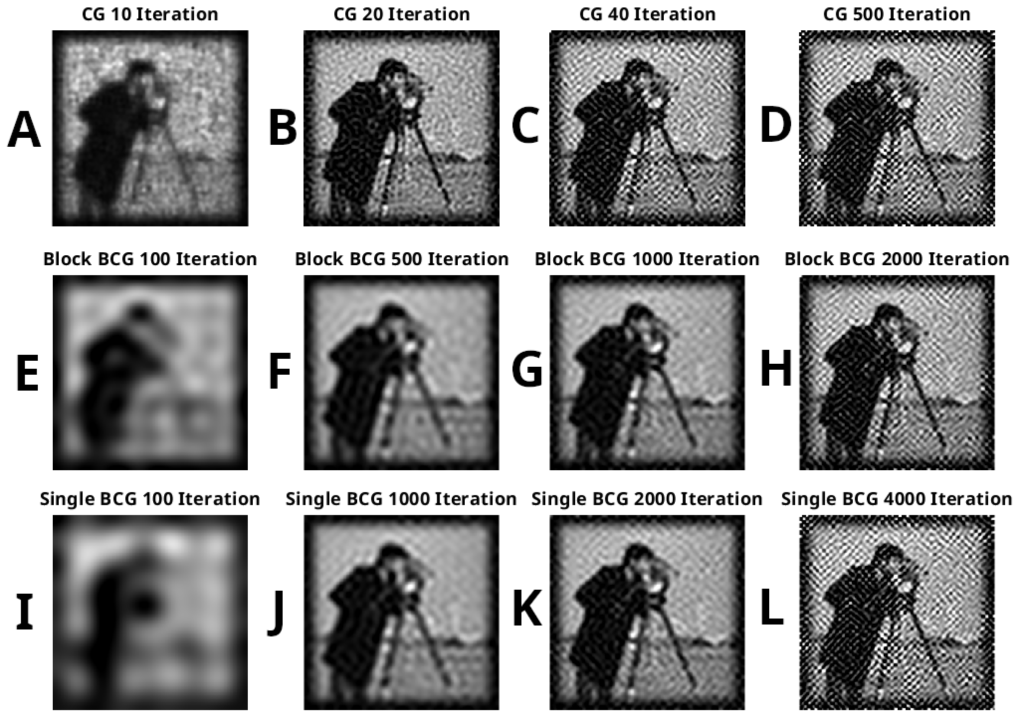

Figure 7. Selected 2D reconstructions at various iterations using the bandlimiting schemes with 10 dB noisy measurements: no step constraints (CG), block-frequency steps (block BCG), and single-2D-DCT-frequency steps (BCG). (**A**–**D**) indicate no step constraints at 10, 20, 40, and 500 iterations, respectively. (**E**–**H**) indicate block-step constraints at 100, 500, 1000, and 2000 iterations, respectively. (**I**–**L**) single-step constraints at 100, 1000, 2000, and 4000 iterations, respectively. In general, results start blurry and resolve more as further iterations are taken; however, noise is also amplified as more iterations are taken. Note that the final iterations shown for each bandlimiting scheme are approximately equivalent.

Comparing the sample 2D reconstructions shown in Figure 7, we can summarize the similarities and differences between the choices of bandlimiting constraints. Without a bandlimited step constraint, features are quickly resolved, reaching a minimum within a few iterations. However, immediately after this minimum, noise amplification overtakes the reconstruction. The single-frequency constrained scheme requires the full 4000 iterations to converge to a similar noisy solution; however, higher-fidelity bandlimited solutions are reached along the way. The block-frequency constraints converge to a similar solution in fewer iterations, but do so at the cost of amplified noise.

The results in Figure 7 additionally show how increased measurement noise reduces each reconstruction's recoverable content, as the balance point between signal recovery and noisy amplification increases in total error and is reached in fewer bandlimiting steps, i.e., at a lower bandwidth. The CG scheme, or no bandlimiting step constraint, appears to reach the lowest minimum total error reconstruction in the 20 dB and 10 dB comparisons. In contrast, in the 0 dB case, the single-step and block-step schemes reach a slightly lower minimum. While a lower reconstruction error in fewer iterations is often desired, note that this minimum is only observable using the synthetic truth image. Additionally, such a minimum solution is difficult to determine without being able to distinguish between signal recovery and noise amplification. By analyzing the bandlimit reconstruction error in Figure 7, we observe that the single and block steps start at higher-fidelity bandlimited reconstructions, but progressively increase in error as noise is amplified in each iteration. Note that all bandlimiting schemes approximately converge to the same reconstruction error at their max iterations. This is expected as the sampling apertures were preconditioned with the same 4000 2D DCT bin bandlimit. This was intentional to showcase that all three bandlimiting schemes approximate the same bandlimited inverse when run to completion. However, the slower convergence of the single- and block-step constraints allows for stopping the reconstruction process before the bandlimit of the preconditioner, thus arriving at a valid bandlimited reconstruction at an assumed SNR threshold or other stopping criteria.

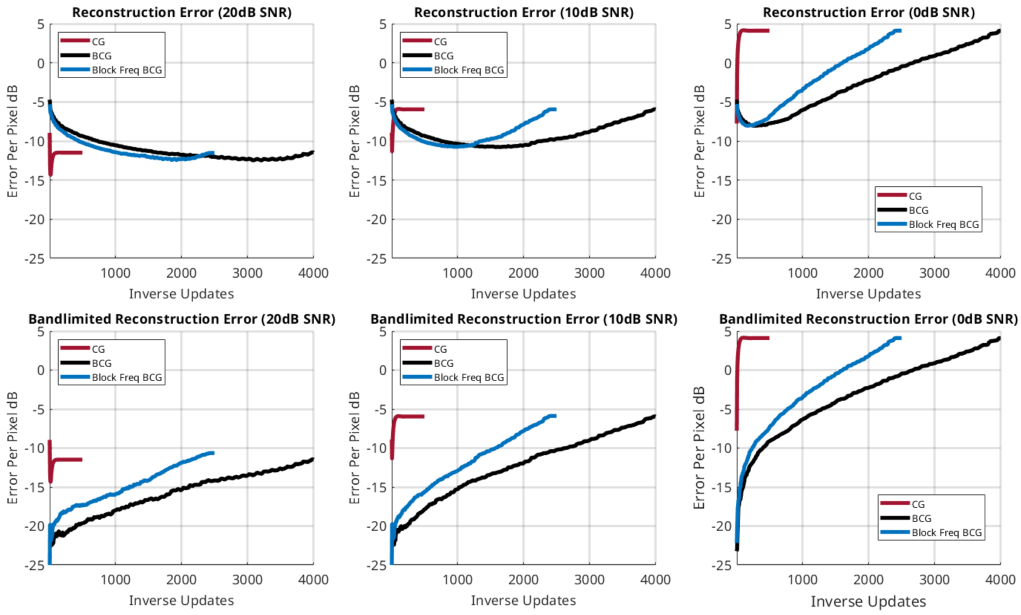

Figure 8. Total and bandlimited reconstruction error results for each iteration of CG, single-frequency BCG, and block-frequency BCG bandlimiting schemes repeated using 20 dB, 10 dB, and 0 dB noisy measurements. In general, the increase in noise tends to cause the minimum point of total reconstruction error to increase and be reached in fewer iterations. Note that all bandlimiting schemes converge to approximately the same reconstruction error at their max iterations. This is expected as the sampling apertures were preconditioned with a 4000 2D DCT bin bandlimit in this simulation.

5. Discussion

While many methods can be used to reconstruct variable aperture measurements, we propose that an iterative bandlimited inverse is preferred for the reconstruction of a bandlimited signal when the bandlimit is unknown. To this end, we have shown how several iterative methods can be constrained to converge towards a bandlimited solution. Additionally, we have shown how a regular aperture deconvolution can initialize the iteration process and reduce the noise amplification of each inversion step. By using progressive bandlimited steps, the estimation process can stop at a valid bandlimited approximation when reaching an expected noise level or SNR.

The bandlimited conjugate gradient descent (BCG) method introduced in this paper is a compromise between traditional conjugate gradient descent and frequency-constrained reconstructions. The choices of initialization and iterative frequency constraint schemes control the rate at which signal content is reconstructed and noise amplified. Using the principles of interactive bandlimited reconstruction discussed in this paper, other existing or future reconstruction algorithms for variable aperture measurements can benefit from initializing the inverse process with a regular aperture deconvolution bandlimiting the error of the reconstruction process and incrementally solving a bandlimited sampling matrix inverse.

While the BCG method can be used to enhance the variable aperture measurements encountered in remote sensing systems, more efficient iterative methods are needed in order to handle higher volumes of measurements, complex sampling systems, and noisy sampling considerations. For example, if tens of thousands of measurements are to be reconstructed using BCG, each iteration requires all previous iteration's conjugate directions. This quickly eats up memory and storage resources. Other iterative methods that do not require such a large iteration history, or methods that reduce the number of measurements such as compressed sensing, may be better suited to high numbers of measurements. Additionally, sampling systems in two or more dimensions may be sensitive to directional sampling errors and can require further frequency constraints to avoid amplifying errors. Furthermore, BCG can be sensitive to noisy environments that contain high spectral components within the bandlimit of reconstruction. Methods that use more than a simple SNR test and other noise suppression techniques may be required for reliable reconstruction.

Regardless of these additional complexities and considerations, the bandlimiting modifications suggested in this paper can be applied to current and future methods to suppress noise content outside the reconstructable bandlimit, speed up the iterative reconstruction process, and progressively reconstruct bandlimited solutions without determining the reconstruction limit beforehand.

Author Contributions: Conceptualization, H.G. and D.G.L.; investigation, H.G.; writing—original draft preparation, H.G.; writing—review and editing, H.G. and D.G.L.; supervision, D.G.L.; funding acquisition, D.G.L. All authors have read and agreed to the published version of the manuscript.

Funding: This research was funded through NASA grant number 80NSSC19K0057.

Data Availability Statement: No new data were created or analyzed in this study. Data sharing is not applicable to this article.

Conflicts of Interest: The authors declare no conflicts of interest.

Abbreviations

The following abbreviations are used in this manuscript:

ART	additive reconstruction technique
BCG	bandlimited conjugate gradient descent
CG	conjugate gradient descent
DFT	discrete Fourier transform
DCT	discrete cosine transform
FFT	fast Fourier transform
FQR	frequency-basis QR reconstruction
SNR	signal-to-noise ratio

Appendix A. Bandlimited Convergence of the Iterative Step Constraint

Starting with the preconditioned and regularized Landweber expression in Equation (4), we can solve for the convergence of the step constraint, assuming λ is sufficiently small to guarantee theoretical convergence, as follows:

$$\hat{\mathbf{x}}_n = \left[\sum_{i=0}^{n} (\mathbf{I} - \lambda \mathbf{HM}^* \mathbf{RM})^i \right] \lambda \mathbf{HM}^* \mathbf{Ry}. \tag{A1}$$

$$\hat{\mathbf{x}}_\infty = (\mathbf{HM}^* \mathbf{RM})^\dagger \mathbf{HM}^* \mathbf{Rz}. \tag{A2}$$

If $\mathbf{H}$ is a Toeplitz or circulant matrix, then $\mathbf{H}^\dagger\mathbf{H} = \mathbf{B}$, where $\mathbf{B}$ is a bandlimited identity matrix ($\mathbf{B}^i = \mathbf{B}$ and $\mathbf{B}^*\mathbf{B} = \mathbf{B}$). This can be shown by diagonalizing $\mathbf{H}$ and $\mathbf{H}^\dagger$ using a discrete Fourier transform matrix [24,25].

Using a Toeplitz $\mathbf{H}$, we can generalize Equation (A2) as to a bandlimited Landweber convergence $\hat{\mathbf{x}}_\infty$, as follows:

$$\hat{\mathbf{x}}_\infty = (\mathbf{BM}^*\mathbf{RM})^\dagger\mathbf{BM}^*\mathbf{Rz}. \tag{A3}$$

In theory, all circulant or Toeplitz $\mathbf{H}$'s converge to a bandlimited solution $\hat{\mathbf{x}}_\infty$ in Equation (A3); however, the noise in $\mathbf{z}$ and the conditioning of $\mathbf{M}$ can prevent this convergence.

To illustrate the benefit of bandlimiting each iteration step, we consider the special case when $\mathbf{M}$ is Toeplitz and $\mathbf{R}$ is the identity matrix. In such a case, we can choose $\mathbf{H} = \mathbf{M}^{*\dagger}$ such that $\lambda\mathbf{HM}^* = \lambda\mathbf{B}$, which reduces Equation (A2) to

$$\begin{aligned}
\hat{\mathbf{x}}_n &= (\mathbf{BM})^\dagger\mathbf{Bz}, \\
\hat{\mathbf{x}}_n &= \left[\sum_{i=0}^{n}(\mathbf{B} - \lambda\mathbf{BM})^i\right]\lambda\mathbf{Bz}, \\
\hat{\mathbf{x}}_{n+1} &= \hat{\mathbf{x}}_n + \lambda\mathbf{B}(\mathbf{z} - \mathbf{M}\hat{\mathbf{x}}_n).
\end{aligned} \tag{A4}$$

In this special case, iteration starts at the bandlimited projection of $\mathbf{z}$ onto $\mathbf{x}$, and each step removes a portion of the bandlimited measurement error, until the projected measurement error is minimized. The benefit of using a bandlimited constraint on each iteration step is that the iteration error is limited to the bandlimit, so the solution can converge before excessive out-of-band noise amplification occurs.

This result can be generalized to any $\mathbf{H}$ by asserting that, through bandlimited interpolation, any projection matrix $\mathbf{U} = \mathbf{H}^\dagger\mathbf{H}$ can be interpolated into a bandlimited identity matrix $\mathbf{B}$ of the same rank. This can be shown by rearranging and interpolating the eigenvectors of $\mathbf{U}$ using a bandlimited interpolation matrix $\mathbb{D}$, i.e., $\mathbb{D}\mathbf{U} = \mathbf{B}$, where an example $\mathbb{D}$ is used in Equation (16).

References

1. Early, D.S.; Long, D.G. Image reconstruction and enhanced resolution imaging from irregular samples. *IEEE Trans. Geosci. Remote Sens.* **2001**, *39*, 291–302. [CrossRef]
2. Strohmer, T. Computationally attractive reconstruction of bandlimited images from irregular samples. *IEEE Trans. Image Process.* **1997**, *6*, 540–548. [CrossRef] [PubMed]
3. Chaubell, J.; Yueh, S.; Entekhabi, D.; Peng, J. Resolution enhancement of SMAP radiometer data using the Backus Gilbert optimum interpolation technique. In Proceedings of the 2016 IEEE International Geoscience and Remote Sensing Symposium (IGARSS), Beijing, China, 10–15 July 2016; pp. 284–287.
4. Alparone, M.; Nunziata, F.; Estatico, C.; Migliaccio, M. A multichannel data fusion method to enhance the spatial resolution of microwave radiometer measurements. *IEEE Trans. Geosci. Remote Sens.* **2020**, *59*, 2213–2221. [CrossRef]
5. He, M.; Yin, X.; Li, Y.; Xu, Q.; Zhou, W.; Lin, M.; Wang, S.; Liu, M.; Wei, Y. Spatial Resolution Enhancement of HY-2B Scanning Microwave Radiometer Low-Frequency Data. *IEEE Trans. Geosci. Remote Sens.* **2023**, *61*, 5302615. [CrossRef]
6. Garrett, H.; Long, D.G. Frequency Constrained QR Signal and Image Reconstruction. *Remote Sens.* 2024, *submitted*.
7. Long, D.G.; Franz, R.O. Band-limited Signal Reconstruction from Irregular Samples with Variable Apertures. *IEEE Trans. Geosci. Remote Sens.* **2015**, *54*, 2424–2436. [CrossRef]
8. Long, D.G. Discrete Band-Limited Signal Reconstruction from Irregular Samples. *IEEE Trans. Geosci. Remote. Sens.* **2020**, *59*, 4033–4043. [CrossRef]
9. Ramlau, R.; Teschke, G.; Zhariy, M. A compressive Landweber iteration for solving ill-posed inverse problems. *Inverse Probl.* **2008**, *24*, 065013. [CrossRef]
10. Nikazad, T. The Use of Landweber Algorithm in Image Reconstruction. Ph.D. Thesis, Matematiska Institutionen, Linköping, Sweden, 2007.

11. Alparone, M.; Nunziata, F.; Estatico, C.; Migliaccio, M. On the use of preconditioners to improve the accuracy and effectiveness of iterative methods to enhance the spatial resolution of radiometer measurements. *IEEE Geosci. Remote Sens. Lett.* **2020**, *18*, 446–450. [CrossRef]
12. Alparone, M.; Nunziata, F.; Estatico, C.; Camps, A.; Park, H.; Migliaccio, M. On the trade-off between enhancement of the spatial resolution and noise amplification in conical-scanning microwave radiometers. *IEEE Trans. Geosci. Remote Sens.* **2022**, *60*,5303714. [CrossRef]
13. Hansen, P.C.; Jørgensen, J.S.; Rasmussen, P.W. Stopping rules for algebraic iterative reconstruction methods in computed tomography. In Proceedings of the 2021 21st International Conference on Computational Science and Its Applications (ICCSA), Cagliari, Italy, 13–16 September 2021; pp. 60–70.
14. Censor, Y. On variable block algebraic reconstruction techniques. In *Mathematical Methods in Tomography, Proceedings of a Conference Held in Oberwolfach, Germany, 5–11 June 1990*; Springer: Berlin/Heidelberg, Germany, 2006; pp. 133–140.
15. Lucy, L.B. An iterative technique for the rectification of observed distributions. *Astron. J.* **1974**, *79*, 745. [CrossRef]
16. Richardson, W.H. Bayesian-based iterative method of image restoration. *JoSA* **1972**, *62*, 55–59. [CrossRef]
17. Shepp, L.A.; Vardi, Y. Maximum likelihood reconstruction for emission tomography. *IEEE Trans. Med. Imaging* **1982**, *1*, 113–122. [CrossRef] [PubMed]
18. Havdiak, M.; Aliaga, J.I.; Iakymchuk, R. Robustness and Accuracy in Pipelined Bi-Conjugate Gradient Stabilized Method: A Comparative Study. *arXiv* **2024**, arXiv:2404.13216.
19. Dehghan, M.; Mohammadi-Arani, R. Generalized product-type methods based on bi-conjugate gradient (GPBiCG) for solving shifted linear systems. *Comput. Appl. Math.* **2017**, *36*, 1591–1606. [CrossRef]
20. Henderson, H.V.; Searle, S.R. On deriving the inverse of a sum of matrices. *Siam Rev.* **1981**, *23*, 53–60. [CrossRef]
21. Fill, J.A.; Fishkind, D.E. The Moore–Penrose Generalized Inverse for Sums of Matrices. *SIAM J. Matrix Anal. Appl.* **2000**, *21*, 629–635. [CrossRef]
22. Lai, S.H.; Vemuri, B.C. Generalized capacitance matrix theorems and algorithm for solving linear systems. *SIAM J. Sci. Comput.* **1998**, *19*, 1024–1045. [CrossRef]
23. Gao, S.; Qu, G. Filter-Based Landweber Iterative Method for Reconstructing The Light Field. *IEEE Access* **2020**, *8*, 138340–138349. [CrossRef]
24. Davis, P.J. *Circulant Matrices*; Wiley: New York, NY, USA, 1979; Volume 2.
25. Gröchenig, K. Irregular sampling, Toeplitz matrices, and the approximation of entire functions of exponential type. *Math. Comput.* **1999**, *68*, 749–765. [CrossRef]